

# Design of phase-switched two-input Kerr flip-flops

Brian A. Daniel and Govind P. Agrawal\*

*The Institute of Optics, University of Rochester, Rochester, New York 14627, USA*

*\*Corresponding author: govind.agrawal@rochester.edu*

Received May 3, 2012; accepted June 10, 2012;  
posted June 13, 2012 (Doc. ID 167916); published August 3, 2012

A two-input configuration for microresonators, exhibiting bistability owing to Kerr nonlinearity, could be used for the realization of optical flip-flops with switching speeds that are not limited by thermal effects. We present design considerations for such devices. The concept of phase switching is explained, and the results of numerical simulations clarify the conditions under which it will succeed. A thermal model is presented and used to understand the influence of the material properties and cavity structure on important operating parameters that will be relevant to any experimental effort to realize the device. © 2012 Optical Society of America

OCIS codes: 130.4815, 190.1450.

## 1. INTRODUCTION

Optical flip-flops are the key elements of all-optical memory and buffering devices. The development of such devices remains in its infancy, even though flip-flops would be valuable in contemporary communication networks. The reason for this is that flip-flops are not yet fast, robust, and low-power enough to be used in the large numbers that these applications demand. The most common means of implementing optical flip-flops is the use of active semiconductor devices. Both semiconductor optical amplifiers [1] and semiconductor lasers [2] have been widely used for this purpose. An alternative would be to use the Kerr effect in a passive, bistable resonator. This second approach has two potential advantages. First, passive flip-flops do not require current injection and devices that require cascading of such elements could be implemented with lower power requirements. Second, the Kerr effect has an almost instantaneous material response. As a result, switching speeds are not limited by the nonlinear medium but by the photon lifetime of the cavity, which can, in principle, be engineered to be as fast as necessary. Implementation of Kerr flip-flops using microresonators has proven to be difficult. When the optical power in a resonator is large, material absorption significantly heats it. The resulting thermo-optic change in refractive index is much stronger and slower than the Kerr effect, and as a result, switching between the “on” and “off” states is limited to microsecond time scales [3–7]. Techniques for getting around this limitation have included cooling the cavity to cryogenic temperatures [8] and using pulsed input fields with temporal durations much smaller than the cavity’s thermal response time [9].

Thermal limitations to the switching speed of an optical flip-flop can also be overcome by using two input fields. A Kerr resonator subjected to two input fields can exhibit a bistability for which the cavity is equally full of light in both stable states [10]. As a result, the steady-state temperature and, hence, the thermal index change would be the same in both states. This thermal index change would be unable to respond on the short time scales during which switching occurs, and it would act as a background change in the refractive index that does not affect the switching speed. In a recent

letter, we demonstrated theoretically that the two-input Kerr flip-flop offers another advantage: it can be switched between its two stable states by pure phase modulations of the input fields [11]. Such phase modulations could be imposed electrically using an electro-optic modulator or optically using cross-phase modulation (XPM) from set and reset pulses, and they may prove simpler to implement than intensity modulations for the purpose of switching.

In this article we consider the design of phase-switched, two-input, Kerr flip-flops in detail. In Section 2 a derivation of the theoretical model used for the analysis is presented. In Section 3 the concept of phase switching is explained. We discuss criteria for appropriate biasing conditions and phase-modulation profiles, which are verified by a comprehensive set of numerical simulations. A thermal model is developed in Section 4 and used to study the influence of material properties and cavity designs on device performance. Methods of estimating important operating parameters such as input power, cavity temperature, and switching speed are presented in order to guide experimental work on this device. The main results of this article are summarized in Section 5.

## 2. THEORETICAL MODEL

A detailed analysis of two-input Kerr bistability was carried out in 1982 by Kaplan and Meystre [10]. They considered two input fields at the same frequency that excite counterpropagating modes in a ring resonator. A steady-state model of the device was developed and used to understand the nature of the solutions under a variety of operating conditions. Haelterman *et al.* later studied a different configuration [12–14] in which a Fabry–Perot cavity was illuminated by two input beams of the same frequency that propagated at different angles. In addition to a steady-state analysis, Haelterman also developed a dynamic model of the two interacting modes and numerically demonstrated flip-flop operation by modulating the intensities of the two input beams [14].

A third configuration for two-input bistability is shown in Fig. 1. In this configuration, the two resonator modes with

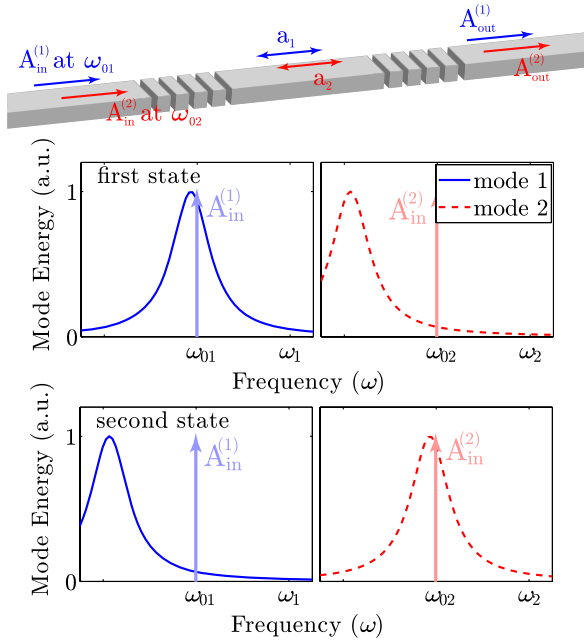


Fig. 1. (Color online) One possible configuration for a two-input Kerr flip-flop. Two input fields at frequencies  $\omega_{01}$  and  $\omega_{02}$  couple to two different resonator modes with resonance frequencies  $\omega_1$  and  $\omega_2$ . In the first state, input field  $A_{\text{in}}^{(1)}$  fills the cavity with light, causing a Kerr-induced redshift of the resonance frequencies. The redshift of the mode 2 resonance is twice as large because the XPM is twice as strong as the SPM. In the second stable state, the roles of the input fields are reversed.

amplitudes  $a_1$  and  $a_2$  propagate in the same directions inside a Fabry–Perot cavity, but they are distinguished by their different resonance frequencies. This type of configuration was considered by Agrawal and Flytzanis [15]. That study was concerned with absorptive bistability near a two-photon material resonance, but the configuration is applicable to Kerr bistability as well. In the Kerr case, the underlying physical mechanism leading to bistable behavior is the same as for the other two configurations. It comes from the fact that XPM from the Kerr effect is twice as strong as self-phase modulation (SPM). Thus, if mode  $a_1$  in Fig. 1 is intense enough so that it causes a Kerr-induced change in its own refractive index by  $\Delta n_{nl}$ , it will cause the refractive index experienced by any light in mode  $a_2$  to change by  $2\Delta n_{nl}$  [16]. As a result of these index changes, both of the modes will experience shifts in their resonance frequencies, and the resonance shift of mode  $a_2$  will be twice as large as the resonance shift of mode  $a_1$ . If the two input fields  $A_{\text{in}}^{(1)}$  and  $A_{\text{in}}^{(2)}$  have the same intensity and are detuned from their initial (low-intensity) resonances by the same amount, this can lead to the existence of two stable states like the ones described conceptually in Fig. 1. In the first state, input field  $A_{\text{in}}^{(1)}$  at frequency  $\omega_{01}$  resonantly excites mode  $a_1$  and fills the cavity with light. This causes input field  $A_{\text{in}}^{(2)}$  at frequency  $\omega_{02}$  to be off resonance so that mode  $a_2$  is only weakly excited. In this state, light at  $\omega_{01}$  is transmitted through the cavity and light at  $\omega_{02}$  is not. In the second state, the roles of the two input fields are reversed and the cavity transmits light at frequency  $\omega_{02}$  but not at  $\omega_{01}$ .

The theoretical model developed in this section describes all three device configurations discussed so far, and it makes no assumptions about the specific structure of the cavity. It is a dynamic model that can be used to describe the switching

process, as well as the steady-state field behavior. The dynamic equations are similar to the ones derived by Haelterman [14] for the angled-beam configuration, and the steady-state equations are similar to the ones derived by Kaplan and Meystre [10] for the ring-resonator configuration. Thus, it can be considered a general theoretical framework that contains previous methods of analysis within it, demonstrating their applicability to a wider range of devices.

### A. Dynamic-Mode Amplitude Equations

The model is based on the dynamic-mode theory of resonators that was developed in [17]. The electric field in the cavity is written as a sum of the two resonant modes that are excited by the input fields

$$\mathbf{E}(\mathbf{r}, t) = \frac{a_1(t)}{\sqrt{N_1}} \mathbf{e}_1(\mathbf{r}) + \frac{a_2(t)}{\sqrt{N_2}} \mathbf{e}_2(\mathbf{r}), \quad (1)$$

where  $\mathbf{e}_k(\mathbf{r})$  is the electric-field profile associated with the  $k$ th mode ( $k = 1, 2$ ) of the resonator. The mode amplitudes are normalized so that  $|a_k(t)|^2$  is the electromagnetic energy stored in mode  $k$  at time  $t$ . The constant  $N_k$  is a normalization factor given by

$$N_k = \frac{1}{2} \int \varepsilon_0 \varepsilon(\mathbf{r}) |\mathbf{e}_k|^2 d^3\mathbf{r}, \quad (2)$$

where the dielectric permittivity  $\varepsilon(\mathbf{r})$  describes the structure of the cavity.

When the medium inside the cavity exhibits the Kerr effect, there is, in addition to the linear response described by the permittivity, a nonlinear response described by the third-order dipole-moment density [16]

$$P_{\mu}^{(3)}(\mathbf{r}, t) = \frac{3\varepsilon_0}{4} \sum_{\alpha, \beta, \gamma} \chi_{\mu\alpha\beta\gamma}^{(3)} E_{\alpha}(\mathbf{r}, t) E_{\beta}^*(\mathbf{r}, t) E_{\gamma}(\mathbf{r}, t), \quad (3)$$

where  $\chi_{\mu\alpha\beta\gamma}^{(3)}$  is the third-order susceptibility tensor. It was shown in [17] that, for an assumed solution of the form (1), Maxwell's equations imply the following equations for the mode amplitudes:

$$\frac{da_k}{dt} = -i\omega_k a_k - \frac{a_k}{2\tau_{\text{ph}}} + \kappa A_{\text{in}}^{(k)}(t) + \frac{i\omega_k}{4\sqrt{N_k}} \int \mathbf{e}_k^* \cdot \mathbf{P}^{(3)} d^3\mathbf{r}, \quad (4)$$

where  $\tau_{\text{ph}}$  is the photon lifetime of the cavity;  $\kappa$  is a coupling coefficient; and  $A_{\text{in}}^{(k)}$  is the input field to mode  $k$ , which is normalized so that  $|A_{\text{in}}^{(k)}|^2$  is its optical power. It is assumed for the sake of simplicity that  $\tau_{\text{ph}}$  and  $\kappa$  are the same for the two modes. Using Eq. (3) in Eq. (4) together with Eq. (1), we obtain the following two coupled nonlinear differential equations:

$$\frac{da_1}{dt} = -i\omega_1 a_1 - \frac{a_1}{2\tau_{\text{ph}}} + \kappa A_{\text{in}}^{(1)}(t) + i(\gamma_{11}|a_1|^2 + 2\gamma_{12}|a_2|^2)a_1, \quad (5)$$

$$\frac{da_2}{dt} = -i\omega_2 a_2 - \frac{a_2}{2\tau_{\text{ph}}} + \kappa A_{\text{in}}^{(2)}(t) + i(\gamma_{22}|a_2|^2 + 2\gamma_{21}|a_1|^2)a_2. \quad (6)$$

In deriving these equations, a number of terms have been neglected. Depending on which device configuration is being considered, there are different justifications for this neglect. For a configuration using two spectrally distinct modes, these additional terms are not frequency matched to the mode resonances, and hence they have a negligible influence on the mode amplitudes. In the case of modes that may have the same resonance frequency but are spatially distinct, such as counterpropagating modes in a ring resonator, these terms are vanishingly small as a result of the spatial phase structure of the modes.

The SPM and XPM terms appearing in Eqs. (5) and (6) depend on a set of four nonlinear parameters given by

$$\gamma_{kl} = \frac{\omega_k n_2 c \eta_{kl}}{n_0^2 (V_k V_l)^{1/2}}. \quad (7)$$

In Eq. (7)  $V_k$  is an *effective mode volume* defined as

$$V_k = \frac{\left( \int \epsilon(\mathbf{r}) |\mathbf{e}^{(k)}|^2 d^3 \mathbf{r} \right)^2}{n_0^4 \int (|\mathbf{e}^{(k)}|^2)^2 d^3 \mathbf{r}}. \quad (8)$$

The parameter  $n_2$  that appears in Eq. (7) is the Kerr coefficient responsible for the intensity dependence of refractive index in the nonlinear medium. In general,  $n_2$  depends on the orientation of the electric field with respect to the crystallographic axes. In practice,  $n_2$  is chosen to be the value for some particular crystallographic direction. The third-order susceptibility  $\chi_c^{(3)}$  in this direction is related to  $n_2$  as [16]

$$\chi_c^{(3)} = \frac{4}{3} \epsilon_0 c n_0^2 n_2, \quad (9)$$

where  $n_0$  is the linear (low-intensity) refractive index of the medium. The parameter  $\eta_{kl}$  that appears in Eq. (7) is a *nonlinear overlap factor* given by

$$\eta_{kl} = \sum_{\mu\alpha\beta\gamma} \frac{\int \chi_{\mu\alpha\beta\gamma}^{(3)} e_\mu^{*(k)} e_\alpha^{(k)} e_\beta^{*(l)} e_\gamma^{(l)} d^3 \mathbf{r}}{\int (|\mathbf{e}^{(k)}|^2)^2 d^3 \mathbf{r} \int (|\mathbf{e}^{(l)}|^2)^2 d^3 \mathbf{r}}. \quad (10)$$

Physically, the nonlinear overlap factors measure how effectively the modes interact through the third-order susceptibility. It is often a good approximation to take  $\eta_{kl} \approx 1$ . It is also often a good approximation to take  $V_k \approx V_{\text{cav}}$ , where  $V_{\text{cav}}$  is the volume of the cavity. If the two input fields additionally have nearly the same frequency, then  $\gamma_{11} \approx \gamma_{22} \approx \gamma_{12} \approx \gamma_{21} = \gamma$ , where

$$\gamma \approx \omega_1 c n_2 / (n_0^2 V_{\text{cav}}). \quad (11)$$

This approximate form of  $\gamma$  will be used throughout the rest of this article.

## B. Steady-State Solutions

Equations (5) and (6) describe the behavior of the resonator for any input-field temporal profiles  $A_{\text{in}}^{(1)}(t)$  and  $A_{\text{in}}^{(2)}(t)$ . For designing an optical flip-flop, we are interested in the stable, steady states of the resonator when two continuous-wave (CW) fields with constant intensities are launched into it. The input fields then take the form

$$A_{\text{in}}^{(k)}(t) = B_k e^{-i\omega_k t}, \quad (12)$$

where  $B_k$  are constants. For such input fields, the steady-state solutions of Eqs. (5) and (6) take the form

$$a_k(t) = b_k e^{-i\omega_k t}. \quad (13)$$

Using Eqs. (12) and (13) in Eqs. (5) and (6), we obtain a pair of algebraic equations for the complex constants  $b_k$ ,

$$[-i(\Delta\omega_k + \gamma|b_k|^2 + 2\gamma|b_{3-k}|^2) + 1/2\tau_{\text{ph}}]b_k = \kappa B_k, \quad (14)$$

where  $\Delta\omega_k = \omega_{0k} - \omega_k$  is the detuning of the  $k$ th input field from resonance. These equations result in the following pair of coupled equations for the mode energies  $E_k = |b_k|^2$ ,

$$[(\Delta\omega_k + \gamma E_k + 2\gamma E_{3-k})^2 + (1/2\tau_{\text{ph}})^2]E_k = |\kappa|^2 P_k, \quad (15)$$

where  $P_k = |B_k|^2$  is the power of the  $k$ th input field. Once a solution is found for the mode energies by solving Eq. (15), Eq. (14) can be used to find the phases of  $b_k$ .

Solving Eq. (15) does not, however, guarantee that the resulting solution represents a physically realizable state of the device. In order to be realizable, it is also necessary that the solution be stable. A stable solution is characterized by its being robust to small perturbations. If a small perturbation is applied to a stable state, it tends to die out and the system remains in that state. In contrast, if a small perturbation is applied to an unstable state, the system evolves away from that state and does not return to it. Stability of various solutions of Eq. (15) can be examined by performing a linear stability analysis of Eqs. (5) and (6), as outlined in Appendix A.

## 3. FLIP-FLOP DESIGN CRITERIA

### A. Biasing Conditions

The available stable states of the flip-flop depend on the power levels and detunings of the two input fields, as indicated by Eq. (15). The flip-flop could be designed such that these properties are different between the two fields, but this would be undesirable. As discussed in Section 1, thermal nonlinearities can be a problem for a flip-flop having different intracavity intensities in its two states. As a result, it is desirable to bias the device symmetrically so that the input fields have the same power and detuning from their respective resonances. In this situation, we can expect a pair of states to exist that exhibit the same intracavity energy, such as those depicted in Fig. 1. Mathematically, these states are found by solving Eq. (15) with the conditions

$$\Delta\omega_1 = \Delta\omega_2 = \Delta\omega_0, \quad (16)$$

$$P_1 = P_2 = P_0, \quad (17)$$

and then examining their stability using the linear stability analysis presented in Appendix A.

Kaplan and Meystre solved a very similar pair of equations when they studied the Kerr interaction of two counterpropagating modes in a ring resonator [10]. We follow their analysis and point out its implications for the biasing conditions of a flip-flop. They found that the solutions of Eq. (15) under

symmetric biasing conditions can be divided into two categories. The first category contains all symmetric solutions, characterized by the equality of their mode energies ( $E_1 = E_2$ ). The second category contains all asymmetric solutions for which  $E_1 \neq E_2$ . Because the biasing conditions are themselves symmetric, the asymmetric solutions come in pairs because the roles of  $E_1$  and  $E_2$  can always be reversed.

The solutions depicted in Fig. 1 for the two states of a flip-flop are a pair of asymmetric solutions. Clearly, it is necessary to choose  $P_0$  and  $\Delta\omega_0$  so that such a pair of solutions exists at that bias point. An ideal bias point will also have the property of supporting no other stable states. If, for example, there were a stable symmetric solution in addition to the asymmetric pair, then the flip-flop might slip into this undesirable state and stop working. Such biasing is clearly not ideal. Figure 2 shows the set of ideal bias points in the  $(\Delta\omega_0, P_0)$  plane, following the analysis of [10]. The solid curve in the figure bounds the set of bias points that support asymmetric solutions. The dashed curve bounds the set of bias points for which multiple symmetric solutions exist. Bias points in this second set are nonideal because one of the symmetric solutions is always found to be stable. Thus, the ideal bias points lie in the shaded region of Fig. 2. The flip-flop can operate at any of these ideal bias points. In the following analysis, as an example, we focus on a particular bias point by choosing  $\Delta\omega_0\tau_{\text{ph}} = -2$  and power  $P_0$  such that  $4\gamma|\kappa|^2\tau_{\text{ph}}^3P_0 = 2$ . The results of our analysis apply qualitatively to other ideal bias points as well. The differences among them are quantitative in nature. They will, for instance, exhibit different extinction ratios between the high and low transmission states of the flip-flop. Additionally, the relative robustness of phase switching will vary among them.

### B. Phase-Modulation Profile

Hopf *et al.* were the first to consider switching of a single-input Kerr resonator through pure phase modulation of the input field [18,19]. They found theoretically that the bistable device could be switched on or off by modulating the input phase on time scales short compared to the photon lifetime of the cavity. More recent studies have considered switching one-input devices by simultaneously modulating both the amplitude and phase of the input field. It was shown in [20] that even high- $Q$  cavities can be switched both on and off in an almost instantaneous manner by coherently combining

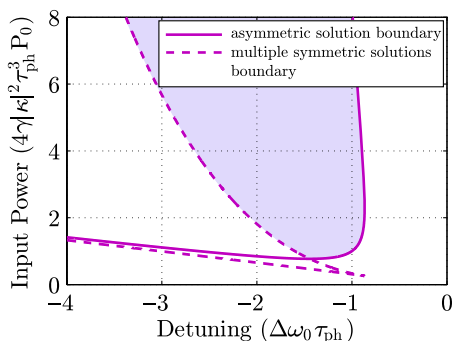


Fig. 2. (Color online) Map of possible bias points when the input fields have the same power  $P_0$  and detuning  $\Delta\omega_0$ . The solid and dashed curves bound regions for which asymmetric solutions exist and multiple symmetric solutions exist, respectively [10]. The ideal bias points lie in the shaded region.

set/reset pulses with the input field at an appropriate relative phase. In [21] it was found that, with appropriate selection of the spectral phase profile of a pulse, its energy can be more efficiently coupled into a cavity, which can be advantageous for switching.

Here, we consider switching of the two-input Kerr resonator by pure phase modulations of the input fields. This phenomenon is modeled by solving Eqs. (5) and (6) with input fields of the form

$$A_{\text{in}}^{(k)}(t) = B_k e^{i\phi_k(t) - i\omega_{0k}t}, \quad (18)$$

where  $\phi_k(t)$  is a time-dependent phase imposed on the field by a control signal. This could be accomplished electrically by using an electro-optic phase modulator, or optically using XPM of an input field by a set or reset pulse. The result of this phase modulation is to temporarily change the detuning of the field's frequency from resonance as

$$\Delta\omega_k(t) = \Delta\omega_{0k} - \frac{d\phi_k}{dt}. \quad (19)$$

If the phase modulation is slow enough for the resonator to respond, then its effect can be understood as temporarily modifying the biasing conditions and, hence, the available stable states toward which the system will evolve.

The phase switching of an optical flip-flop can be understood using Fig. 3, where we plot the available stable states as a function of detuning ( $\Delta\omega_2\tau_{\text{ph}}$ ) of input field 2, while the detuning of input field 1 and the power levels of both fields are kept constant at the bias point:  $\Delta\omega_1\tau_{\text{ph}} = -2$  and  $4\gamma|\kappa|^2\tau_{\text{ph}}^3P_0 = 2$ . The transmission of mode  $k$  is calculated using [22]

$$T_k = |\kappa a_k / A_{\text{in}}^{(k)}|^2. \quad (20)$$

We assume that resonator loss is dominated by the two couplers so that  $|\kappa|^2 = 1/2\tau_{\text{ph}}$ . If a phase modulation with a positive derivative is applied to input field 2 so that  $\Delta\omega_2\tau_{\text{ph}} < -2$ , then Fig. 3 indicates that transmission of both fields will drop to a low state. When the phase modulation ceases and  $\Delta\omega_2\tau_{\text{ph}}$  comes back to its bias value of  $-2$ , it is unclear what state the system will end up in. This situation is clearly not of interest for switching. If, on the other hand, a phase modulation with a negative derivative is applied to input field 2 so that  $\Delta\omega_2\tau_{\text{ph}} > -2$ , the device enters the shaded region in Fig. 3 where the only available state is one for which the

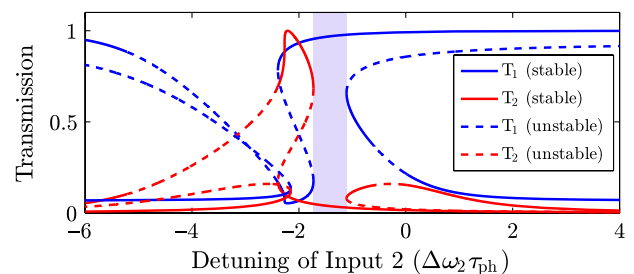


Fig. 3. (Color online) Stable and unstable states of the device when the detuning of input field 2 deviates from the initial biasing at  $\Delta\omega_2\tau_{\text{ph}} = \Delta\omega_1\tau_{\text{ph}} = -2$ . The shaded region indicates where the flip-flop can be switched by modulating the phase of input field 2.

transmission of field 1 is high but the transmission of field 2 is low. Thus, if the transmission of field 2 is initially in the high state, such a phase modulation can force the device to flip. In an analogous way, a subsequent phase modulation of input field 1 can cause the device to flop.

In practice, it is necessary to turn off the signal that applies the modulation after a short time interval. As an example, we consider Gaussian phase shifts of the form

$$\phi_k(t) = \phi_0 e^{-(t-t_p)^2/T_0^2}, \quad (21)$$

where  $\phi_0$  is the maximum phase shift occurring at time  $t_p$ , and  $T_0$  is a measure of the temporal duration of the phase modulation. Positive values of  $\phi_0$  allow for switching to occur. The reason for this is that the trailing edge of the modulation determines the final state of the device after the signal is gone. Thus, even though a positive value of  $\phi_0$  increases the phase over the leading edge of the signal, which does not necessarily switch the device, the trailing edge creates a decreasing phase shift that can switch the device under the appropriate conditions. Maximum detuning can be derived using Eqs. (19) and (21) and is found to be

$$\Delta\omega_k^{\max} \approx \Delta\omega_0 + 0.86\phi_0/T_0. \quad (22)$$

In order for the device to switch, it is necessary that this maximum detuning be large enough to drive the device into the shaded switching region in Fig. 3. This necessity imposes a constraint on the maximum phase shift  $\phi_0$  and temporal duration  $T_0$ . Noting that  $\Delta\omega_2$  should increase by about  $1/\tau_{\text{ph}}$ , we obtain the following approximate criterion for switching of the flip-flop:

$$\phi_0 > T_0/\tau_{\text{ph}}. \quad (23)$$

Equation (23) is not sufficient for a phase modulation to switch the device. It is also necessary that the modulation occur over a long enough temporal duration that the resonator can respond. This leads to the following second criterion:

$$T_0 > \tau_{\text{ph}}. \quad (24)$$

The approximate criteria for the phase-modulation parameters in Eqs. (23) and (24) are verified by rigorous numerical solutions of Eqs. (5) and (6). The input fields are taken to be of the form of Eq. (18) with phase modulations of the form of Eq. (21). The flip-flop is biased using two CW fields with detunings  $\Delta\omega_0\tau_{\text{ph}} = -2$  and powers given by  $4\gamma|\kappa|^2\tau_{\text{ph}}^3P_0 = 2$ . As in Fig. 3, the resonator loss is assumed to be dominated by coupling so that  $|\kappa|^2 = 1/2\tau_{\text{ph}}$ .

Initially, the flip-flop is in a state for which the transmission of input field 2 is high and the transmission of input field 1 is low. The impact of phase switching is then studied by applying three phase modulations of the form given in Eq. (21) at times  $t_p = 0, 50\tau_{\text{ph}}$ , and  $100\tau_{\text{ph}}$ . The first modulation is applied to input field 2 (set operation) and the remaining two to field 1 (reset operations).

We consider first the role of the maximum phase shift  $\phi_0$  and fix the duration of the phase modulation at  $T_0 = 2\tau_{\text{ph}}$ . Figure 4 shows the switching behavior for four values of  $\phi_0$  ranging from 2 to  $2\pi$ . When  $\phi_0 = 2$ , the set operation fails, indicating that this value of  $\phi_0$  is not large enough for the

flip-flop to work. However, when  $\phi_0$  is slightly increased to 2.3, both the set and reset operations succeed, and the flip-flop turns on and off as expected. Note that this switching threshold agrees well with the criterion in Eq. (23). Note also that when two reset operations occur in succession, the second does not change the state of the device.

One may ask if there is an upper limit on the value of  $\phi_0$ . As the maximum phase shift is further increased to  $\pi$  and  $2\pi$ , as shown in Fig. 4, the set and reset operations continue to succeed. Further simulations indicate that switching continues to succeed for maximum phase shifts up to  $\phi_0 \approx 9$  but fails for still larger values. This upper limit occurs when the maximum detuning is  $\Delta\omega_k^{\max}\tau_{\text{ph}} \approx 1.9$  according to Eq. (22). This implies that phase switching is even more robust than can be ascertained from Fig. 3, and it succeeds when phase modulations shift the detuning of field 2 well to the right of the shaded ideal-switching region shown there. From a practical perspective, the important point is that there is a wide range of  $\phi_0$  values over which phase switching succeeds.

We consider next the role of the duration  $T_0$  of the phase modulation. For this purpose, we fix the maximum phase shift at a value of  $\phi_0 = \pi$ . Figure 5 shows the switching behavior for four values of the duration  $T_0$ . When  $T_0 = \tau_{\text{ph}}/2$ , the set operation fails, indicating that the phase is changed so fast that the resonator is unable to respond to it. When the duration is increased to  $T_0 = \tau_{\text{ph}}$ , the set and reset operations succeed. Note that this switching threshold agrees well with the criterion in Eq. (24). As  $T_0$  is increased to  $4\tau_{\text{ph}}$ , the switching continues to succeed. However, if  $T_0$  is further increased to  $5\tau_{\text{ph}}$ , the set operation fails. The reason for this failure can be understood by noting that the criterion in Eq. (23) does not hold for the values of  $T_0$  and  $\phi_0$  used in this last case.

#### 4. CAVITY DESIGN CONSIDERATIONS

The analysis has so far assumed only one kind of material nonlinearity: the Kerr effect. There are always, however, other effects associated with a given material system. Semiconductors often exhibit nonlinear loss mechanisms such as two-photon absorption and subsequent free-carrier absorption, which are likely to prevent the device from functioning. If optical fields were employed with photon energies below the half-bandgap, this problem could be avoided so that the large Kerr nonlinearity of semiconductors could be leveraged for low-power operation. Other candidate material systems include silicon dioxide and silicon nitride. Neither of these exhibit significant nonlinear absorption near the  $1.55\ \mu\text{m}$  wavelength, and fabrication of resonators is technologically well developed for both of these materials [3,4,6–9,23].

There is one type of material nonlinearity that cannot be avoided. Even if the medium is nearly transparent, some optical power is always lost through material absorption. As discussed in Section 1, this absorption inevitably heats the cavity and changes its refractive index via the thermo-optic effect. For a two-input flip-flop, this thermal index change does not affect the switching process because it has the same value in both of the stable states and responds on a time scale much longer than that required for switching. It does, however, present two practical problems. First, if the temperature change is large enough it can physically damage or destroy the resonator. Second, it presents a technical challenge for turning on the device. The reason for this can be understood as follows:

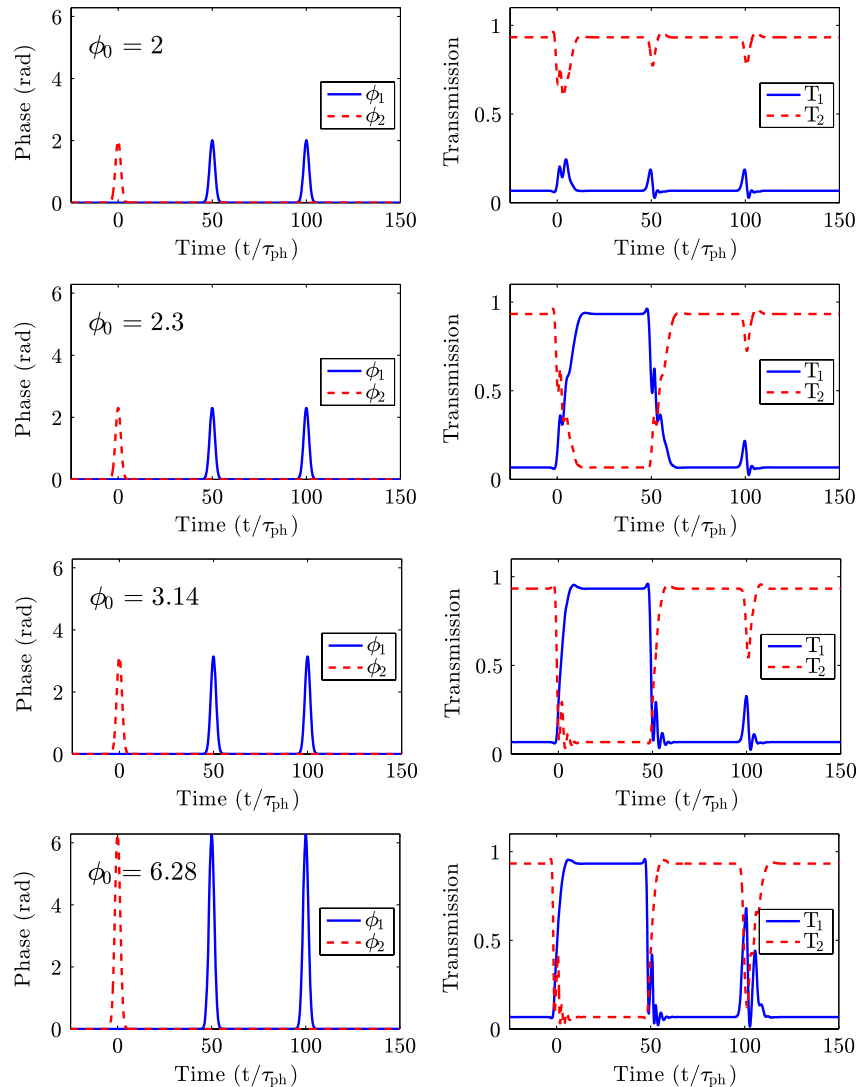


Fig. 4. (Color online) Phase switching for four different values of the maximum phase shift  $\phi_0$  when the duration of the modulation is fixed at  $T_0 = 2\tau_{\text{ph}}$ . Temporal variations of the phase (left) and transmission (right) are shown for input fields 1 (solid blue curves) and 2 (dashed red curves).

in the cold-cavity state, before the input fields are turned on (i.e., when  $A_{\text{in}}^{(1)} = A_{\text{in}}^{(2)} = 0$ ) the  $k$ th mode's resonance frequency is  $\omega_k$ . In the operation mode, when both lasers are on and bistability has been achieved, the new resonance frequency is  $\omega_k' = \omega_k + \Delta\omega_T + \Delta\omega_{\text{Kerr}}^{(k)}$ , where  $\Delta\omega_T$  is the resonance shift from the cavity's change in temperature, and  $\Delta\omega_{\text{Kerr}}^{(k)}$  is the resonance shift from the Kerr effect. When the lasers are first turned on, they might be so far from the cold-cavity resonances that neither input field is able to couple into the cavity and heat it up. As a result, simply turning the lasers on will not transition the device from the cold-cavity state into operation mode. In order to do this, it may be necessary to come up with a means of heating the cavity. This could be done using a thermo-electric temperature controller, or by sweeping the frequency of one of the input fields to "drag" the cold-cavity resonances close to the operation frequency. Either way it will be desirable that  $\Delta\omega_T$  be as small as possible compared to  $\Delta\omega_{\text{Kerr}}^{(k)}$ . Its value will depend on the materials used to make the device as well as on the geometric structure of the resonator.

### A. Simple Thermal Model

To analyze the influence of material properties on the temperature shifts that are responsible for  $\Delta\omega_T$ , we develop a thermal model of the device. Consider the influence of a weak material absorption on the cavity's photon lifetime. The overall photon lifetime is given by [22]

$$\frac{1}{\tau_{\text{ph}}} = \frac{1}{\tau_{\text{ph}}^{\text{ab}}} + \frac{1}{\tau_{\text{ph}}^{\text{sc}}} + \frac{1}{\tau_{\text{ph}}^{\text{e}}}, \quad (25)$$

where  $\tau_{\text{ph}}^{\text{ab}}$ ,  $\tau_{\text{ph}}^{\text{sc}}$ , and  $\tau_{\text{ph}}^{\text{e}}$  represent contributions from material absorption, scattering losses, and coupling losses, respectively. Using the perturbative theory of Section 1, it can be shown that the contribution from material absorption is given by

$$\frac{1}{\tau_{\text{ph}}^{\text{ab}}} \approx \frac{c\alpha_m}{n_0}, \quad (26)$$

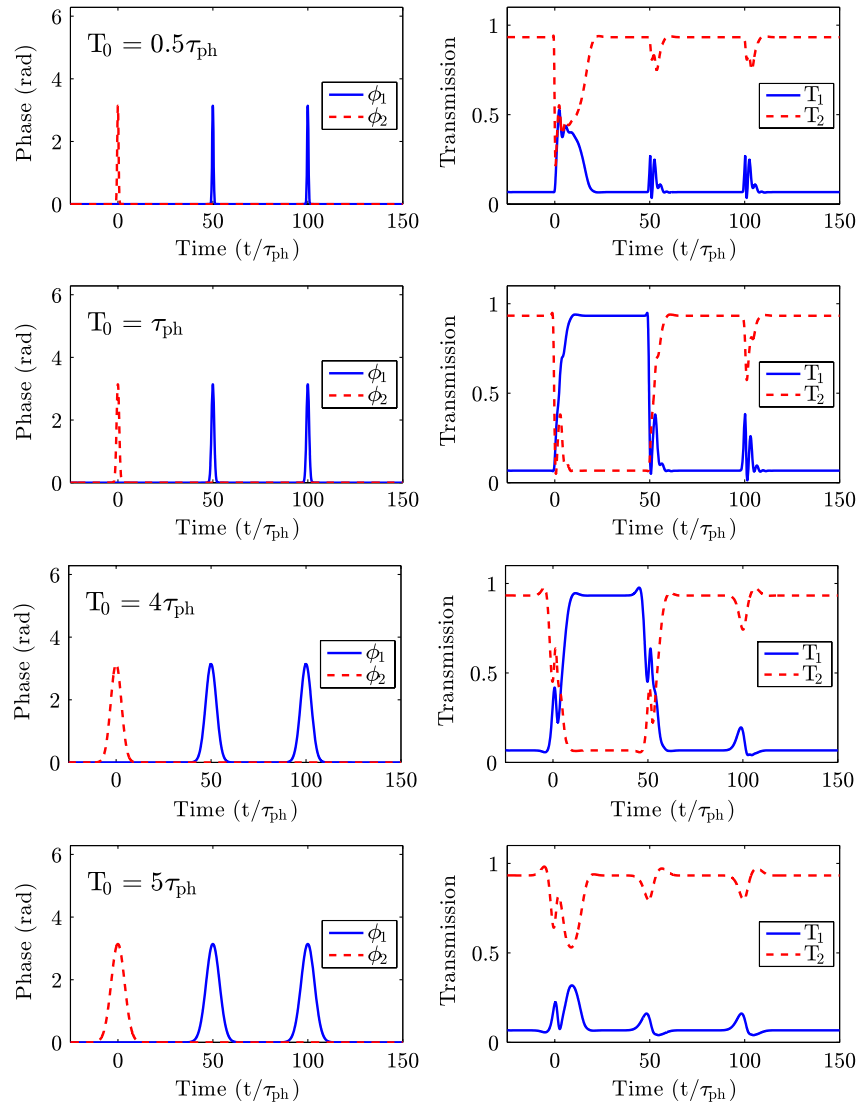


Fig. 5. (Color online) Phase switching for four different values of  $T_0$  when the maximum phase shift is fixed at  $\phi_0 = \pi$ . Temporal variations of the phase (left) and transmission (right) are shown for input fields 1 (solid blue curves) and 2 (dashed red curves).

where it has been assumed that the optical field is primarily confined to a single material with absorption coefficient  $\alpha_m$  and refractive index  $n_0$ . By considering the rate at which electromagnetic energy is lost owing to this absorption, we find that the thermal energy  $\Delta U_T$  stored in the cavity changes with time as

$$\frac{d\Delta U_T}{dt} = \frac{c\alpha_m}{n_0} (|a_1|^2 + |a_2|^2) - \frac{\Delta U_T}{\tau_T}, \quad (27)$$

where  $\tau_T$  is the thermal lifetime.

The thermal energy is related to the thermo-optic change in refractive index as

$$\Delta n_T = \frac{(\partial n/\partial T)\Delta U_T}{\rho C_\rho V_{\text{cav}}}, \quad (28)$$

where  $\partial n/\partial T$  is the medium's thermo-optic coefficient,  $C_\rho$  is its specific heat capacity, and  $\rho$  is its density. Equations (27) and (28) indicate that  $\Delta n_T$  evolves with time as

$$\frac{d\Delta n_T}{dt} = \frac{(\partial n/\partial T)c\alpha_m}{n_0\rho C_\rho V_{\text{cav}}} (|a_1|^2 + |a_2|^2) - \frac{\Delta n_T}{\tau_T}. \quad (29)$$

Equation (29) describes how the optical field in the resonator influences the thermal index shift. The influence of the index shift  $\Delta n_T$  on the mode amplitudes is incorporated in the dynamic equations (5) and (6) by adding another term so that they become [17]

$$\begin{aligned} \frac{da_k}{dt} = & -i\omega_k a_k - \frac{a_k}{2\tau_{\text{ph}}} + \kappa A_{\text{in}}^{(k)}(t) + i\gamma(|a_k|^2 + 2|a_{3-k}|^2)a_k \\ & + i\omega_k \frac{\Delta n_T}{n_0} a_k. \end{aligned} \quad (30)$$

The last term in this equation represents a thermally induced shift of the cavity's resonance frequency by an amount  $\Delta\omega_T = -\omega_k \Delta n_T/n_0$ .

The thermal resonance shift of the device in operation mode can be calculated by considering the steady-state solution of Eqs. (29) and (30), and it is found to be

$$\Delta\omega_T \approx -\frac{\omega_k \tau_T c \alpha_m (\partial n / \partial T)}{n_0^2 \rho C_\rho V_{\text{cav}}} E_{\text{cav}}, \quad (31)$$

where  $E_{\text{cav}} = E_1 + E_2$  is the optical energy stored in the cavity. Because the optical field in the cavity is dominated by one mode in each of the states (e.g., the  $k$ th mode), the optical energy can be approximated by that of this dominant mode ( $E_{\text{cav}} \approx E_k$ ). With this approximation, the Kerr-induced resonance shift of the dominant mode can be shown from Eq. (30) to be

$$\Delta\omega_{\text{Kerr}} \approx -\frac{\omega_1 c n_2}{n_0^2 V_{\text{cav}}} E_{\text{cav}}, \quad (32)$$

where Eq. (11) has been used for  $\gamma$ . Equations (31) and (32) imply that the ratio of the thermal resonance shift to the Kerr-induced resonance shift is

$$\Upsilon_T = \left| \frac{\Delta\omega_T}{\Delta\omega_{\text{Kerr}}} \right| = \frac{\tau_T \alpha_m (\partial n / \partial T)}{\rho C_\rho n_2}. \quad (33)$$

Because  $\Upsilon_T$  depends primarily on material properties, it can be seen as a figure of merit for comparing candidate material systems out of which to construct the resonator. The only term in Eq. (33) that is not purely a material parameter is  $\tau_T$ , which measures how quickly the cavity dissipates heat with the surrounding environment and has some dependence on its geometric structure. Active cooling of the cavity can reduce the effective value of  $\tau_T$  and improve the figure of merit. Models that show the influence of material properties and cavity structure on  $\tau_T$  have also been developed in [4,7] for different types of cavities.

### B. Influence of Resonator Structure

The resonator structure affects two parameters, the quality factor ( $Q$ ) and cavity volume ( $V_{\text{cav}}$ ), that influence device performance. Both of these need to be engineered so that the flip-flop can be made with a low enough bias power, low enough operating temperature, and fast enough speed.

The power of each of the input fields at the bias point that we have used in the preceding analysis is given by  $2\gamma\tau_{\text{ph}}^2 P_0 = 2$  when the resonator loss is dominated by coupling. Using this expression and Eq. (11) for  $\gamma$  leads to the following estimate of the required bias power:

$$P_0 \approx \left( \frac{V_{\text{cav}}}{Q^2} \right) \frac{\omega_1 n_0^2}{c n_2}. \quad (34)$$

This relation shows that the required power is proportional to the volume of the cavity. This makes sense because a smaller volume will require less input power to achieve the same intracavity intensity and therefore the same Kerr-induced resonance shift. Equation (34) also indicates that the needed bias power depends inversely on  $Q^2$ . Physically, one factor of  $Q$  results from the fact that a larger quality factor implies a proportionately higher cavity enhancement of the optical power of an input field. The other factor of  $Q$  comes from the fact that a larger quality factor implies a proportionately smaller bandwidth of the cavity resonance. Bistable operation is achieved when the Kerr-induced shift of a resonance is comparable to its bandwidth. Because the Kerr-induced shift is

proportional to the optical power inside the cavity, a smaller bandwidth results in a proportionately lower requirement for the bias power.

The temperature shift of the cavity when the flip-flop becomes operational is also important because too much heating can damage it. The temperature shift can be calculated by solving Eq. (27) for the steady-state thermal energy in the cavity and using the relation  $\Delta T = \Delta U_T / \rho C_\rho V_{\text{cav}}$ , where  $\Delta T$  is the temperature shift. The result is

$$\Delta T \approx \left( \frac{1}{Q} \right) \frac{2\tau_T \alpha_m n_0}{n_2 \rho C_\rho}, \quad (35)$$

where the steady-state intracavity energy has been approximated by  $E_{\text{cav}} \approx 2/\gamma\tau_{\text{ph}}$  and Eq. (11) has been used for  $\gamma$ . Equation (35) indicates that the operating temperature depends inversely on the quality factor, but that it does not depend on the cavity volume. The independence on cavity volume results from the fact that the required power scales with  $V_{\text{cav}}$  [Eq. (34)]. Thus, the intracavity intensity and, hence, the operating temperature do not depend on  $V_{\text{cav}}$  when the device is appropriately engineered. The inverse dependence of the operating temperature on  $Q$  occurs because a smaller Kerr-induced frequency shift is needed if the resonator has a higher quality factor. The Kerr-induced resonance shift and the thermal resonance shift are directly proportional [Eq. (33)], and the thermal shift is directly proportional to the change in temperature. A higher  $Q$  therefore implies a proportionately smaller temperature shift.

It might be concluded from Eqs. (34) and (35) that it is desirable to design the cavity to have the largest  $Q$  possible. However, this is not necessarily the case because the quality factor also determines the device's switching speed. Numerical simulations in Fig. 4 indicate that the temporal duration over which the flip-flop switches between states can be as small as  $T_{\text{sw}} = 5\tau_{\text{ph}}$ . Noting that  $Q = \omega_1 \tau_{\text{ph}}$ , a higher quality factor results in a longer switching time.

## 5. CONCLUSIONS

The phase-switched two-input Kerr flip-flop has been analyzed in detail in this article. The appropriate biasing conditions, including input-field power levels and detunings from resonance, were clarified. Intuitive criteria for phase modulations of the input fields to set/reset the flip-flop were found and verified by a comprehensive set of numerical simulations. A thermal model of the device was also developed, and it clarified the influence of material properties and cavity structure on device performance. The model was used to derive a figure of merit for comparing the relative severity of thermal effects between potential material systems, as well as a number of important operating parameters that will be relevant to any experimental effort to demonstrate the device. It is the hope of the authors that the analysis of this article will equip other investigators for such an effort. It would not only be an interesting endeavor, because two-input Kerr bistability has not been experimentally demonstrated to our knowledge, but it would also be a relevant one because the proposed flip-flop has potential to be used for all-optical signal processing applications.

## APPENDIX A: LINEAR STABILITY ANALYSIS

Consider the solutions of Eq. (14) for the mode amplitudes  $b_k$ . These correspond to steady-state solutions of Eqs. (5) and (6) of the form of Eq. (13). Now imagine that the fields are slightly perturbed, such as would occur regularly in a real device. After the perturbation the solutions of Eqs. (5) and (6) can be written in the form

$$a_k(t) = b_k[1 + c_k(t)]e^{-i\omega_k t}, \quad (\text{A1})$$

where  $|c_k| \ll 1$ . Using this form in Eqs. (5) and (6), the fact that  $b_k$  satisfy Eq. (14), and neglecting all terms higher than the first order in  $c_k$ , we obtain a system of four differential equations that describe how the perturbation evolves in time. We can write them in matrix form as

$$\frac{d\mathbf{c}}{dt} = i\gamma \overleftrightarrow{S}\mathbf{c}, \quad (\text{A2})$$

where  $\mathbf{c} = [c_1 \ c_2 \ c_1^* \ c_2^*]^T$  is a column vector and the matrix  $\overleftrightarrow{S}$  is given by

$$\overleftrightarrow{S} = \begin{pmatrix} q_1 & 2E_2 & E_1 & 2E_2 \\ 2E_1 & q_2 & 2E_1 & E_2 \\ -E_1 & -2E_2 & -q_1^* & -2E_2 \\ -2E_1 & -E_2 & -2E_1 & -q_2^* \end{pmatrix}, \quad (\text{A3})$$

where  $q_k = 2(E_1 + E_2) + (\Delta\omega_k + i/2\tau_{\text{ph}})/\gamma$ .

Any solution of Eq. (A2) can be written as a linear combination of its eigenmodes. The eigenmodes are constructed from the eigenvectors and corresponding eigenvalues of the matrix  $\overleftrightarrow{S}$ , which satisfy

$$\overleftrightarrow{S}\mathbf{c}_m = \lambda_m \mathbf{c}_m. \quad (\text{A4})$$

The eigenmode solutions are given by  $\mathbf{c}_m e^{i\gamma\lambda_m t}$ . If any of these eigensolutions grow exponentially in time, then it is possible for a small perturbation to drive the modes away from the steady-state solutions  $b_k$ , indicating that they are unstable. If, on the other hand, all of the eigensolutions decay exponentially in time, then the solutions  $b_k$  are stable. This occurs when all of the eigenvalues  $\lambda_m$  satisfy

$$\text{Im}\{\lambda_m\} > 0, \quad (\text{A5})$$

which is the criterion used to determine the stability of steady-state solutions in this article.

## REFERENCES

1. D. N. Maywar, K. P. Solomon, and G. P. Agrawal, "Remote optical control of an optical flip-flop," *Opt. Lett.* **32**, 3260–3262 (2007).
2. L. Liu, R. Kumar, K. Huybrechts, T. Spuesens, G. Roelkens, E. Geluk, T. de Vries, P. Regreny, D. V. Thourhout, R. Baets, and G. Morthier, "An ultra-small, low-power, all-optical flip-flop memory on a silicon chip," *Nat. Photon.* **4**, 182–187 (2010).
3. V. B. Braginsky, M. L. Gorodetsky, and V. S. Ilchenko, "Quality-factor and nonlinear properties of optical whispering-gallery modes," *Phys. Lett. A* **137**, 393–397 (1989).
4. V. S. Ilchenko and M. L. Gorodetsky, "Thermal nonlinear effects in optical whispering gallery microresonators," *Laser Phys.* **2**, 1004–1009 (1992).
5. V. R. Almeida and M. Lipson, "Optical bistability on a silicon chip," *Opt. Lett.* **29**, 2387–2389 (2004).
6. H. Rokhsari and K. J. Vahala, "Observation of Kerr nonlinearity in microcavities at room temperature," *Opt. Lett.* **30**, 427–429 (2005).
7. K. Ikeda, R. E. Saperstein, N. Alic, and Y. Fainman, "Thermal and Kerr nonlinear properties of plasma-deposited silicon nitride/silicon dioxide waveguides," *Opt. Express* **16**, 12987–12994 (2008).
8. F. Treussart, V. S. Ilchenko, J.-F. Roch, J. Hare, V. Lefèvre-Seguin, J.-M. Raimond, and S. Haroche, "Evidence for intrinsic Kerr bistability of high-Q microsphere resonators in superfluid helium," *Eur. Phys. J. D* **1**, 235–238 (1998).
9. M. Pöllinger and A. Rauschenbeutel, "All-optical signal processing at ultra-low powers in bottle microresonators using the Kerr effect," *Opt. Express* **18**, 17764–17775 (2010).
10. A. E. Kaplan and P. Meystre, "Directionally asymmetrical bistability in a symmetrically pumped nonlinear ring interferometer," *Opt. Commun.* **40**, 229–232 (1982).
11. B. A. Daniel and G. P. Agrawal, "Phase-switched all-optical flip-flops using two-input bistable resonators," *IEEE Photon. Technol. Lett.* **24**, 479–481 (2012).
12. M. Haelterman, P. Mandel, J. Danckaert, H. Thienpont, and I. Veretennicoff, "Two-beam nonlinear Fabry–Perot transmission characteristics," *Opt. Commun.* **74**, 238–244 (1989).
13. M. Haelterman and P. Mandel, "Pitchfork bifurcation using a two-beam nonlinear Fabry–Perot interferometer: an analytical study," *Opt. Lett.* **15**, 1412–1414 (1990).
14. M. Haelterman, "All-optical set-reset flip-flop operation in the nonlinear Fabry–Perot interferometer," *Opt. Commun.* **86**, 189–191 (1991).
15. G. P. Agrawal and C. Flytzanis, "Two-photon double-beam optical bistability," *Phys. Rev. Lett.* **44**, 1058–1061 (1980).
16. R. W. Boyd, *Nonlinear Optics*, 3rd ed. (Academic, 2008).
17. B. A. Daniel, D. N. Maywar, and G. P. Agrawal, "Dynamic mode theory of optical resonators undergoing refractive index changes," *J. Opt. Soc. Am. B* **28**, 2207–2215 (2011).
18. F. A. Hopf, P. Meystre, P. D. Drummond, and D. F. Walls, "Anomalous switching in dispersive optical bistability," *Opt. Commun.* **31**, 245–250 (1979).
19. F. A. Hopf and P. Meystre, "Phase-switching of a dispersive non-linear interferometer," *Opt. Commun.* **33**, 225–230 (1980).
20. H. Kawashima, Y. Tanaka, N. Ikeda, Y. Sugimoto, T. Hasama, and H. Ishikawa, "Numerical study of impulsive switching of bistable states in nonlinear etalons," *IEEE Photon. Technol. Lett.* **19**, 913–915 (2007).
21. S. Sandhu, M. L. Povinelli, and S. Fan, "Enhancing optical switching with coherent control," *Appl. Phys. Lett.* **96**, 231108 (2010).
22. H. A. Haus, *Waves and Fields in Optoelectronics* (Prentice-Hall, 1984).
23. M. Tien, J. F. Bauters, M. J. R. Heck, D. T. Spencer, D. J. Blumenthal, and J. E. Bowers, "Ultra-high quality factor planar Si<sub>3</sub>N<sub>4</sub> ring resonators on Si substrates," *Opt. Express* **19**, 13551–13556 (2011).